



Calorimetric approach to establishing thermokinetics for cosmeceutical benzoyl peroxides containing metal ions

An-Chi Huang¹ · Fu-Chung Liao^{2,3} · Chung-Fu Huang⁴ · Yan Tang¹ · Yang Zhang⁵ · Chi-Min Shu⁶ · Zhi-Xiang Xing¹ · Jun-Cheng Jiang¹ · Wen-Ying Hsieh²

Received: 15 June 2020 / Accepted: 20 February 2021 / Published online: 23 March 2021
© Akadémiai Kiadó, Budapest, Hungary 2021

Abstract

Cosmeceutical products have improved over the years; however, the explosions and fire accidents in cosmeceutical factories worldwide have not ceased. Literature researches on this genre of potential risk have been seldom published. Cosmeceutical benzoyl peroxide (CBPO) is usually used on facial products, especially for acne treatment. The thermal stability of CBPO with additions and calorimetric technology is utilized to obtain the thermal stability and reaction characteristics. Depending on the experimental thermal stability parameters, apparent activation energy was calculated by various integral and differential kinetic models. Uniting the isoconversional kinetic analysis and numerical simulation of the isothermal condition can better realize the decomposition characteristics and potential process risk. Dozens of milligrams of CBPO were dunked with 10,000 ppm of Cu, Fe, and Zn to inspect the exothermal behavior. The findings can be a reference for the essential safety parameters and customer safety design for the database.

Keywords Fire accidents · Thermal stability · Reaction characteristics · Kinetic model · Isoconversional kinetic · Numerical simulation

List of symbols

ΔH_d Heat of decomposition (J g^{-1})
 A Frequency factor (1 s^{-1})

✉ Chung-Fu Huang
huangchungfu@gmail.com

✉ Yan Tang
tycd@cczu.edu.cn

✉ Chi-Min Shu
shucm@yuntech.edu.tw

¹ School of Environmental and Safety Engineering, Changzhou University, Changzhou 213164, Jiangsu, China

² Graduate School of Technological and Vocational Education, National Yunlin University of Science and Technology (YunTech), Yunlin 64002, Taiwan, ROC

³ Petrochemical Business Division Lin Yuan Petrochemical Plant, Chinese Petroleum Corporation Corporation, Kaoshiung 83245, Taiwan, ROC

⁴ School of Environmental and Chemical Engineering, Zhaoqing College, Zhaoqing 526061, Guangdong, China

⁵ School of Emergency Management and Safety Engineering, China University of Mining and Technology (Beijing), Beijing 100083, China

⁶ Department of Safety, Health, and Environmental Engineering, YunTech, Yunlin 64002, Taiwan, ROC

C Constant (dimensionless)
 C_s Constant for Starink method (dimensionless)
 D Correction coefficient for apparent activation energy (dimensionless)
 E_a Apparent activation energy (kJ mol^{-1})
 $f(\alpha)$ Differential form of reaction mechanism function (dimensionless)
 $g(\alpha)$ Integral form of reaction mechanism function (dimensionless)
 i The power of absolute temperature in Starink (dimensionless)
 $p(x)$ Integral temperature
 R Universal gas constant [$8.314 \text{ J (mol K)}^{-1}$]
 R^2 Coefficient of determination (dimensionless)
 $SADT$ Self-accelerating decomposition temperature ($^{\circ}\text{C}$)
 t Time (min)
 T Absolute temperature (K)
 T_0 Apparent onset temperature ($^{\circ}\text{C}$)
 TCL Time to conversion limit (day)
 TMR_{iso} Time to the maximum rate at isothermal conditions (h)
 T_f Final reaction temperature ($^{\circ}\text{C}$)
 T_p Peak temperature ($^{\circ}\text{C}$)

Greek letters

α	Extent of conversion (dimensionless)
β	Heating rate ($^{\circ}\text{C min}^{-1}$)

Introduction

Cosmeceutical benzoyl peroxide (CBPO) is used to permeate the pores and eliminate propionibacterium acnes, which causes pimples on the human skin, especially for teenagers. CBPO is essentially different from other antibiotics, with moderate excitability and no drug resistance. Moreover, CBPO is more effective than prescription drugs, such as oral and topical antibiotics. Hence, it is the most effective over-the-counter bactericide currently used to treat acne [1, 2].

Cosmeceutical factories usually implement numerous chemicals in different production processes. However, because of the potential hazardous risk from operator errors, essential material hazards, or incompatibility of production lines, cosmeceutical factory explosion accidents and news are intermittently reported [3, 4].

According to dangerous chemical properties, organic peroxides face challenges from storage, transportation, usage, and waste stream treatments. An inappropriate operation may result in an incompatible chemical reaction and therefore cause a thermal accident [5, 6]. The references report the potential thermal risk of organic peroxides. If the rate of heat removal is sustained lower than that of heat generation, the inner thermal system exceedingly produces a runaway reaction [7, 8]. The hazardous features of lower concentration organic peroxide have also been indicated; the exothermic onset temperature (T_0) of organic peroxide samples does not change with the concentration change. Even though the concentration is low to 10 mass%, the detectable exothermic behaviors are digitized [9, 10].

As classical organic peroxide, CBPO has undoubtedly hazardous traits. Furthermore, the medical concentration of CBPO on treatment is usually lower to 10 mass% [11, 12]. The self-accelerating decomposition temperature (SADT) value of lower concentration CBPO is merely 48 $^{\circ}\text{C}$. Moreover, the reference evaluated the time to conversion limit (TCL) by Thermal Safety Software; when the subject sample was stored at 27.5 $^{\circ}\text{C}$, TCL was 21 days [9].

Several incompatible reactions were caused by the contact between organic peroxides and metal ions. Different organic peroxides have incompatible materials. When cumene hydroperoxide contacted iron ion, the time to the maximum rate at isothermal conditions (TMR_{iso}) was reduced from 9.49 to 0.37 h at 110 $^{\circ}\text{C}$ [13, 14]. Impurities like metal ions are commonly present during the process, usage, storage, and transportation. Therefore, to ensure the incompatible reaction between CBPO and metal ions, the safety parameters, including SADT and TMR_{iso} , were calculated.

The findings of this study indicate the potential thermal risk of contact between CBPO and various metal ions. Moreover, the composition of thermokinetics happening during the decomposition and runaway reaction was revealed. Multiple thermokinetic reactions were determined as autocatalysis reactions, followed by n th order reactions. This paper also provides the safe design considerations of the CBPO production line and the theoretical and practical knowledge of future product development.

Experimental

Sample preparation

The original concentration CBPO in the sample preparation was 75.0 mass%, which is white crystals. The 75.0 mass% CBPO was supplied by Gu-Tek International Industry Corporation, Taichung, Taiwan. We selected 1.0, 2.5, 5.0, and 10.0 mass% CBPO as the target samples. The 16 sets of CBPO test samples were well prepared, saved in sample dishes, and refrigerated from 3.0 to 5.0 $^{\circ}\text{C}$. The prepared samples did not further process before being transfused hooked on the DSC receptacle. Therefore, the original concentrated CBPO was diluted with methyl salicylate.

Moreover, we selected Cu, Fe, and Zn as potentially incompatible metal ions. The metal ions were purchased from Showa Kako Corp. (Osaka, Japan) in powder form. Each concentration of CBPO was separately formulated into four samples, which were the original samples, added with Cu, Fe, and Zn. Simulating the impurities amount like metal ions are small in the real situation, the different CBPO samples and metal ions mass ration were dispensed as only 1% [15].

Differential scanning calorimetry

The DSC currently on the market can be divided into heat flux DSC and power compensation DSC. The DSC we selected to examine the heat flow change during the decomposition of 16 sets of samples was PerkinElmer DSC 8500. PerkinElmer DSC 8500 (Shelton, CT, USA) belongs to power compensation DSC, which has high energy precision and accuracy with small furnace mass and can reach balance quickly [16, 17]. DSC 8500 was employed to examine thermal behavior characteristic in the entire process when the samples were heated from room temperature to 200.0 $^{\circ}\text{C}$. We chose the part of the heating range determined by the thermogravimetry experiments [18, 19].

According to the suggestion of DSC operation parameters for calculating and establishing thermokinetic models, the heating rates we used were 1.0, 2.0, 4.0, 6.0, and 8.0 $^{\circ}\text{C min}^{-1}$ [20, 21]. The heating rate selection strictly

follows that the multiple heating rates should be adopted, and the ratio of the maximum β ($8.0\text{ }^{\circ}\text{C min}^{-1}$) to the minimum β ($1.0\text{ }^{\circ}\text{C min}^{-1}$) should not be < 5 [22, 23]. For the DSC test container, we selected $25\text{ }\mu\text{L}$ aluminum crucible for all the sets of samples. The selected aluminum crucible can be used for standard DSC testing up to $640\text{ }^{\circ}\text{C}$, for solid, liquid, and powder samples, and can provide excellent DSC performance [15]. The amount of four different concentrations of CBPO mixed with different metal ions examined for each heat flow experiment was $5.30 \pm 0.17\text{ mg}$. The experiment atmosphere selected was nitrogen; when the nitrogen was turned on, the carrier gas flow rate was set to about 20.0 mL min^{-1} [24]. Given experimental reproducibility, four CBPO sample concentrations and those containing metal ions samples were repeatedly executed three times [25].

Results and discussion

DSC experiments of CBPO mixed with metal ions

We performed thermal stability tests, which were three metal ions mixed four different low concentration CBPO at DSC

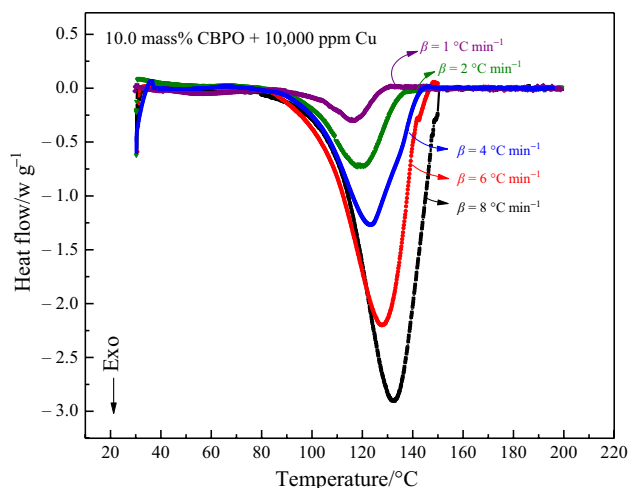


Fig. 1 DSC curves of heat flow versus temperature for 10.0 mass% CBPO mixed with 10,000 ppm Cu at various heating rates

experiments. The DSC curves of heat flow versus temperature for 10.0 mass% CBPO mixed with 10,000 ppm Cu at the heating rates of 1.0, 2.0, 4.0, 6.0, and $8.0\text{ }^{\circ}\text{C min}^{-1}$, as shown in Fig. 1. At the beginning of the furnace heating, the instrument recorded a little noise, which did not affect the calculation for the heat of decomposition (ΔH_d) of the test samples. The origin heat flow baselines displayed an indefinite value with the heating rate changing. The DSC curves baseline was restructured to better present a comparison. Because the tested samples were dissolved as dilution liquid, the endothermic reaction was not expected to occur. When CBPO decomposed, the benzoic acid, benzene, and biphenyl were released.

Meanwhile, the exothermic peak shaved shriller when the heating rate was higher. As listed in Table 1, the initial exothermic onset temperature (T_0), which is defined as the temperature at which the heat that is released by a reaction cannot be removed from the reactor, started at approximately $91.85 \pm 7.25\text{ }^{\circ}\text{C}$ and ended at ca. $99.26 \pm 0.96\text{ }^{\circ}\text{C}$. The heat flow of exothermal direction was downward in DSC 8500 illustration. Therefore, the peak temperature (T_p) appeared at the lowest point in each DSC curve, as shown in Fig. 1. For 10.0 mass% CBPO mixed with 10,000 ppm Cu DSC tests, the T_p occurred at $124.38 \pm 7.26\text{ }^{\circ}\text{C}$, which is congenial to the literature and increased by degrees of heating rates [10].

As listed in Table 1, the entire decomposition of four concentrations CBPO mixed with 10,000 ppm Cu presented a similar value for T_0 , T_p , and final temperature (T_f). However, because of the concentration difference of CBPO, the primary influence of thermal stability is reflected in ΔH_d . The ΔH_d of 1.0, 2.5, 5.0, and 10.0 mass% CBPO mixed with 10,000 ppm Cu were distributed from $17.23 \pm 3.48\text{ J g}^{-1}$ to $60.26 \pm 17.73\text{ J g}^{-1}$. Although the values of ΔH_d for each concentration of CBPO did not grow in multiples proportionally with the concentration of CBPO, the lower concentration could affect the ΔH_d value with a considerable impact. Moreover, the T_p is the indicative parameter to calculate the E_a ; the coefficient of variation (CV) of T_p was listed in Table 1 to present the experiments' reliability. Tables 2 and 3 present the thermal stability parameters of lower concentrated CBPO mixed with 10,000 ppm Fe and mixed with 10,000 ppm Zn in DSC experiments. For CBPO mixed with 10,000 ppm Fe, the primary thermal stability parameters

Table 1 Thermal behavior characteristics of lower concentrated CBPO added Cu analyzed via DSC

CBPO concentration/mass%	Mass/mg	$T_0/^{\circ}\text{C}$	$T_p/^{\circ}\text{C}$	CV of T_p	$T_f/^{\circ}\text{C}$	$\Delta H_d/\text{J g}^{-1}$
1.0	5.18 ± 0.20	92.08 ± 3.53	125.96 ± 7.4	5.9%	145.78 ± 6.29	17.23 ± 3.48
2.5	5.04 ± 0.03	97.81 ± 5.42	125.47 ± 6.93	5.5%	144.30 ± 7.62	28.30 ± 1.18
5.0	5.25 ± 0.18	91.85 ± 7.25	124.38 ± 7.26	5.8%	144.83 ± 8.70	58.37 ± 1.22
10.0	5.12 ± 0.08	99.26 ± 0.96	124.59 ± 5.73	4.6%	142.47 ± 8.56	60.26 ± 17.73

Number of samples = 5

Table 2 Thermal behavior characteristics of lower concentrated CBPO added with Fe analyzed via DSC

CBPO concentration/mass%	Mass/mg	$T_0/^\circ\text{C}$	$T_p/^\circ\text{C}$	CV of T_p	$T_f/^\circ\text{C}$	$\Delta H_d/\text{J g}^{-1}$
1.0	5.12 ± 0.13	90.94 ± 6.24	126.07 ± 8.26	6.6%	148.05 ± 5.15	14.47 ± 1.35
2.5	5.26 ± 0.16	93.31 ± 3.17	125.42 ± 7.07	5.6%	144.20 ± 7.90	29.69 ± 0.97
5.0	5.24 ± 0.17	87.71 ± 2.07	124.33 ± 7.54	6.1%	146.10 ± 8.52	63.18 ± 1.91
10.0	5.31 ± 0.11	86.71 ± 1.57	123.44 ± 7.90	6.4%	140.35 ± 9.42	77.34 ± 23.25

Number of samples = 5

Table 3 Thermal behavior characteristics of lower concentrated CBPO added with Zn analyzed via DSC

CBPO concentration/mass%	Mass/mg	$T_0/^\circ\text{C}$	$T_p/^\circ\text{C}$	CV of T_p	$T_f/^\circ\text{C}$	$\Delta H_d/\text{J g}^{-1}$
1.0	5.44 ± 0.28	79.90 ± 2.15	119.05 ± 6.86	5.8%	143.18 ± 1.77	26.68 ± 22.25
2.5	5.65 ± 0.17	90.29 ± 1.36	126.10 ± 6.63	5.3%	141.95 ± 2.37	14.81 ± 10.88
5.0	5.10 ± 0.07	85.89 ± 4.36	126.78 ± 7.31	5.8%	147.04 ± 9.51	34.77 ± 3.00
10.0	5.22 ± 0.12	91.28 ± 2.54	126.19 ± 7.99	6.3%	145.48 ± 10.14	55.22 ± 7.34

Number of samples = 5

did not make much difference in T_0 , T_p , and T_f with the data listed in Table 1. Note that the ΔH_d of 1.0 mass% CBPO mixed with 10,000 ppm Fe was lower than that of 1.0 mass% CBPO mixed with 10,000 ppm Cu. Nevertheless, the ΔH_d of 10.0 mass% CBPO mixed with 10,000 ppm Fe detected as $77.34 \pm 23.25 \text{ J g}^{-1}$ was even higher than that of 10.0 mass% CBPO mixed with 10,000 ppm Cu.

In Table 3, the data show an irregular relationship for ΔH_d of different concentrated CBPO mixed with 10,000 ppm Zn. As attributed to the crystallization reaction, it occurred during storage, which Zn ion had crystallized with CBPO. Therefore, the CBPO samples with Zn ion crystallization reaction cannot quantify the ΔH_d accurately. The T_0 , T_p , and T_f of CBPO mixed with 10,000 ppm Zn can still be detectable given that the values were similar to that of CBPO mixed with 10,000 ppm Cu and CBPO mixed with 10,000 ppm Fe. Compared with the pure CBPO, the T_0 of CBPO mixed with metal ions was postponed, the reaction can be determined as a typical reaction [9].

Isoconversional kinetic analysis

To establish the thermokinetic parameters in any part of the reaction, we utilized Friedman kinetic method, a famous model-free kinetic model, to extrapolate the apparent activation energy (E_a). The Friedman model is as follows [22, 26]:

$$\frac{d\alpha}{dt} = A(\alpha) \exp\left[-\frac{E_a(\alpha)}{RT(t)}\right] f(\alpha) \quad (1)$$

$$A'(\alpha) = A(\alpha) f(\alpha) \quad (2)$$

$$\frac{d\alpha}{dt} = A'(\alpha) \exp\left[-\frac{E_a(\alpha)}{RT(t)}\right] \quad (3)$$

$$t_a = \int_0^t dt = \int_{\alpha_0}^{\alpha} \frac{d\alpha}{A'(\alpha) \exp\left[-\frac{E_a(\alpha)}{RT(t)}\right]} \quad (4)$$

$$\ln\left(\frac{d\alpha}{dt}\right) = \ln(A'(\alpha)) - \frac{E_a(\alpha)}{RT(t)} \quad (5)$$

where A is a pre-exponential factor, E_a is the apparent activation energy. The values of A and E_a will change with the temperature change. The model linearizes them to simplify the equation. The rate at which the reaction rate increases with increasing temperature is related to its E_a value. Within the same temperature range, the smaller the E_a reaction is, the faster the heating rate will increase, and the increase in E_a value will decrease the heating rate. $f(\alpha)$ is the reaction model, R is the universal gas constant ($8.314 \text{ J mol}^{-1} \text{ K}^{-1}$), T is the absolute temperature, t is the time, and α is the extent of conversion.

The Flynn–Wall–Ozawa (FWO) isoconversional method is frequently adopted to scrutinize the hazardous materials as the integral methods. The FWO kinetic model was used to diagram the E_a value of any part of reaction progress as the comparisons between the calculations of results by Friedman kinetic model. The FWO kinetic method is usually used to calculate the E_a value. One of the advantages of the FWO kinetic method is that it does not require knowing the reaction mechanism in advance and can avoid errors caused by different reaction mechanisms. We used integral temperature $p(x)$, which was obtained from Doyle's approximation [27]:

$$\ln p(x) = -5.331 - 1.0516x \quad (6)$$

where $p(x)$ is the integral temperature value. Using Eq. (6), FWO kinetic model can be expressed as Eq. (7) [28, 29]:

$$\begin{aligned} \ln(\beta_1) + 1.0516 \left(\frac{E_a}{RT_{p1}} \right) &= \ln(\beta_2) + 1.0516 \left(\frac{E_a}{RT_{p2}} \right) \\ &= \ln(\beta_3) + 1.0516 \left(\frac{E_a}{RT_{p3}} \right) = \dots \end{aligned} \quad (7)$$

where β_1 , β_2 , and β_3 , are the heating rates, T_{p1} , T_{p2} , and T_{p3} are the peak temperatures corresponding to each heating rate.

Freidman and FWO methods were adopted to calculate the E_a values to compare with the decomposition situation at any reaction progress during different concentrations of CBPO mixed with metal ions. We selected two sets of representative experiments as a diagram for isoconversional kinetic analysis. Figure 2 shows the E_a and R^2 values versus reaction progress compared to 10.0 mass% CBPO with 10,000 ppm Cu between calculations using Freidman and FWO method. Using Freidman method results, the E_a value started at 147.37 kJ mol⁻¹ and ended at 300.06 kJ mol⁻¹; the R^2 continued to maintain a value approaching 1.0 but became lower α of 0.95. At the middle of reaction progress, the E_a value was 190.20 kJ mol⁻¹. Using the FWO method result, the E_a value started at 74.12 kJ mol⁻¹ and ended at 205.49 kJ mol⁻¹; the completion of reaction progress accompanied the R^2 value increase. We assumed that the maximum reaction rate occurred at α of 0.5, the E_a value was 94.12 kJ mol⁻¹, and the R^2 value was 0.94.

Fig. 2 E_a and R^2 values versus reaction progress comparison of 10.0 mass% CBPO with 10,000 ppm Cu between calculation using Freidman and FWO methods

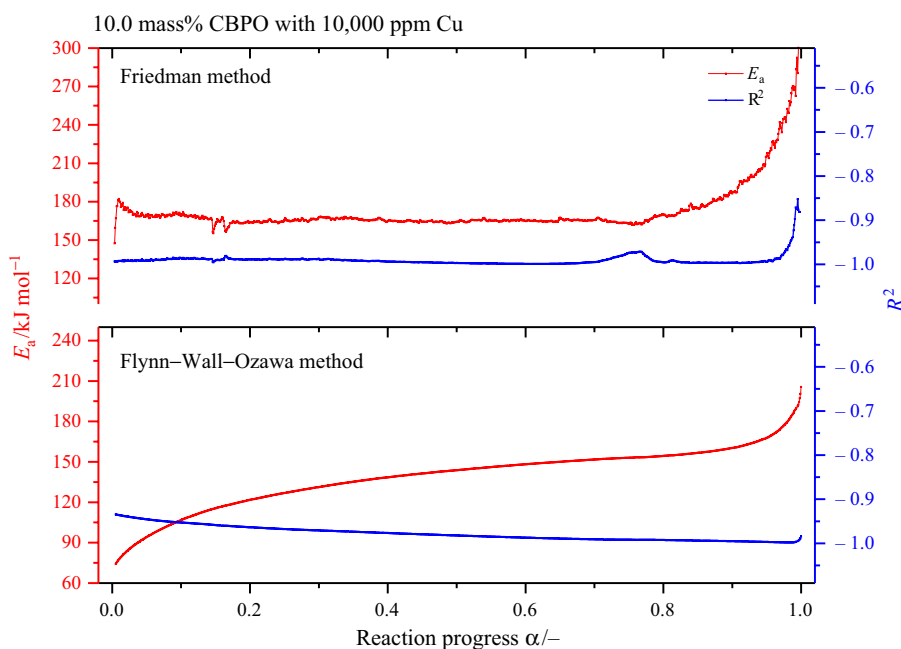


Figure 3 exhibits the E_a and the R^2 values versus reaction progress comparison of 5.0 mass% CBPO with 10,000 ppm Fe between calculations using Freidman and FWO methods. The average values of E_a and R^2 in using the Freidman method were 123.61 kJ mol⁻¹ and 0.99, respectively. When the reaction progress proceeded to 0.5, the E_a value was 143.82 kJ mol⁻¹. In this set of experiments, the FWO method's calculation was comparable to that using the Freidman method; the E_a value started at a higher value and gradually decreased as the reaction proceeded. In calculating 5.0 mass% CBPO with 10,000 ppm Fe using the FWO method, the average values of E_a and R^2 were 145.72 kJ mol⁻¹ and 0.99, respectively. When the reaction proceeded halfway, the E_a value was 133.73 kJ mol⁻¹.

Kissinger method analysis for CBPO

To verify the Friedman method and FWO method calculations' reliability, we used the Kissinger method to duplicate the calculation findings. From Murray and White's approximation to approach the integral temperature $p(x)$, the Kissinger method was developed. Using the approximation, $p(x)$ can be expressed as Eq. (8) [30]:

$$p(x) = \frac{e(-x)}{x^2} \quad (8)$$

Combined with the integral method, the Kissinger kinetic method was transcribed as [31]:

Fig. 3 E_a and R^2 values versus reaction progress comparison of 5.0 mass% CBPO with 10,000 ppm Fe between calculation using Friedman and FWO methods

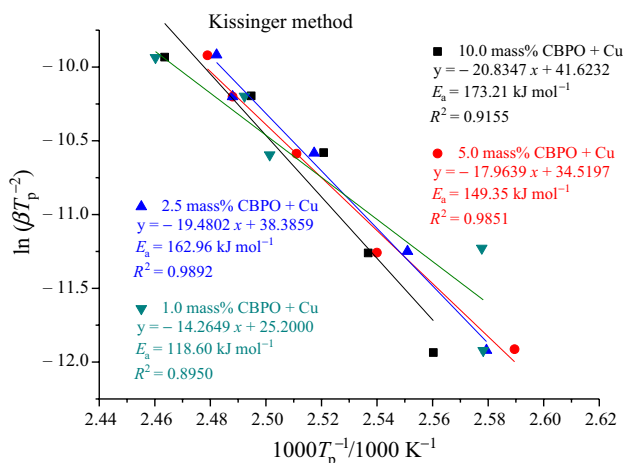
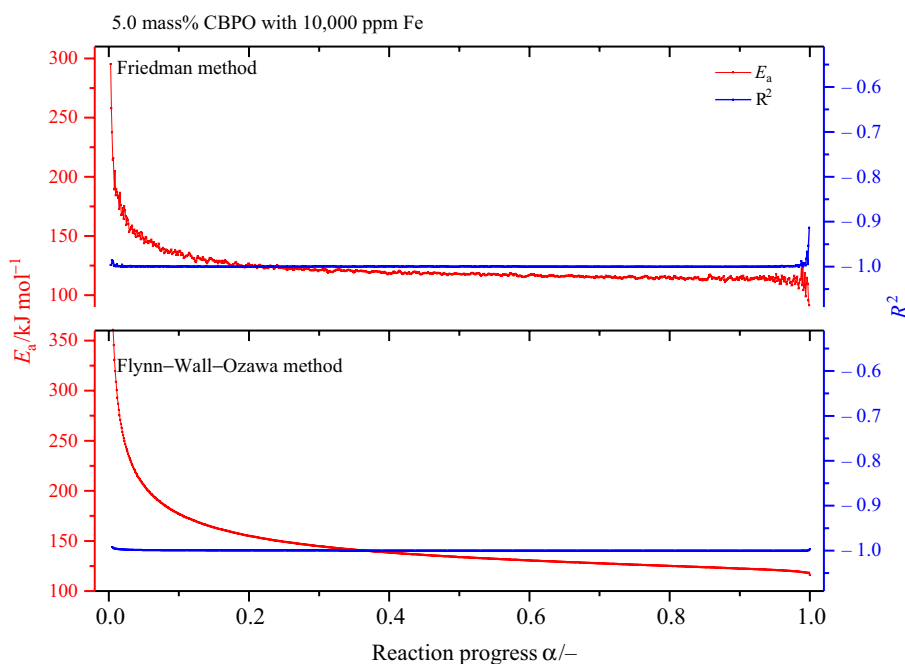


Fig. 4 Plots of $\ln(\beta T_p^{-2})$ versus $1000 T_p^{-1}$ of 1.0, 2.5, 5.0, and 10.0 mass% CBPO with 10,000 ppm Cu under the heating rates of several heating rates

$$\ln\left(\frac{\beta}{T_p^2}\right) = \ln\left[\frac{AR}{E_a g(\alpha)}\right] - \frac{E_a}{RT_p} \quad (9)$$

where $g(\alpha)$ is an integral form of reaction mechanism function. We can obtain the E_a value through the plot of $\ln(\beta T_p^{-2})$ versus T_p^{-1} . The T_p value was assumed as the peak temperature, which is 0.5 in α . As shown in Fig. 4, 1.0, 2.5, 5.0, and 10.0 mass% CBPO with 10,000 ppm Cu under the heating rates of 1.0, 2.0, 4.0, 6.0, and 8.0 °C min⁻¹. The value range of E_a calculated using the Kissinger method was

from 118.60 to 173.21 kJ mol⁻¹; the value of R^2 was from 0.8950 to 0.9851.

Starink method analysis for CBPO

Even though the Friedman kinetic method, FWO kinetic method, and Kissinger kinetic method are the typical model-free models, we further employed the Starink method to calculate E_a to diagnose the thermokinetic results. Based on the transform from Eq. (9), the Starink method can be expressed as Eq. (10):

$$\ln\left(\frac{\beta}{T_i}\right) = C_s - C\left(\frac{E_a}{RT}\right) \quad (10)$$

where β is the heating rate, C_s is the constant, i and C are the approximate values obtained from integral temperature. In the calculation, i and C were appointed as 1.80 and 1.004, respectively. Consequently, the E_a analysis charts using the Starink kinetic method were according to the plot of $\ln(\beta T_p^{-1.8})$ versus $1000 T^{-1}$. The Starink method was recommended to estimate the E_a value accurately [27]. Therefore, in this experimental study, the Starink method was undoubtedly used to describe the experimental data better than the Kissinger method. Figure 5 illustrates the E_a analysis graphs of four sets of CBPO nonisothermal experiments using the Starink method. The range of E_a value is from 109.63 to 142.03 kJ mol⁻¹. The value of R^2 is at least 0.9036, but the highest was only 0.9787. The results revealed that the linear fitting using these model-free methods was stable but not accurate enough in this case (Table 4).

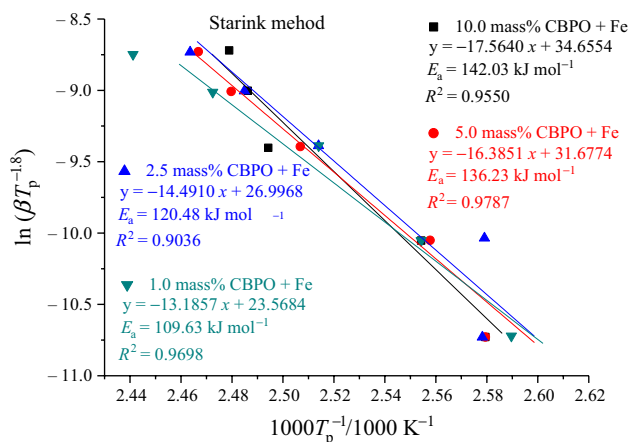


Fig. 5 Plots of $\ln(\beta T_p^{-1.8})$ versus $1000 T_p^{-1}$ of 1.0, 2.5, 5.0, and 10.0 mass% CBPO with 10,000 ppm Fe under the heating rates of several heating rates

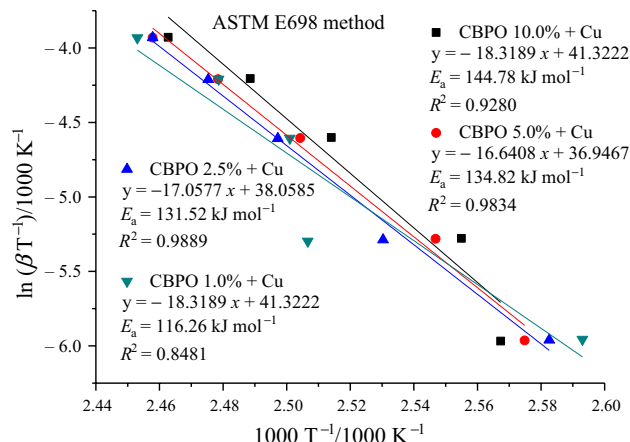


Fig. 6 Graphs used for determining the E_a value of 1.0, 2.5, 5.0, and 10.0 mass% CBPO with 10,000 ppm Cu, using ASTM E698 method

Table 4 E_a determination for various concentrated CBPO and its mixtures using ASTM E698 method

CBPO concentra- tion/mass%	Mixtures			
	Pure	Cu	Fe	Zn
1.0	128.87	116.26	110.56	54.00
2.5	125.38	131.96	130.02	99.39
5.0	129.57	125.92	121.05	126.46
10.0	135.75	158.53	112.63	113.04

Number of samples = 5

American Society for Testing and Materials (ASTM) E698 method

ASTM E698 method can be designated by the Arrhenius equation and general rate law. The main adopted parameters of ASTM E698 were DSC and the FWO method. This method can be utilized to reveal the safety concern of hazardous materials based on the limitation in which several heating rates were in the range from 1.0 to 10.0 °C min⁻¹ [32]. ASTM E698 method can be stated as Eq. (11):

$$E \cong -2.19R \frac{d \log_{10} \beta}{d(1/T)} \tag{11}$$

$$D = -d \frac{\ln \rho(x)}{dx} \tag{12}$$

$$\rho(x) = (x + 2)^{-1} (x^{-1}) (e^{-x}) \tag{13}$$

Using Eqs. (11)–(13), E_a can be calculated as follows:

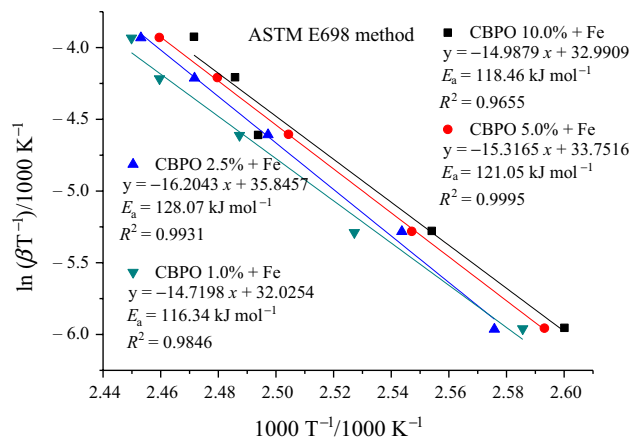


Fig. 7 Graphs used for determining the E_a value of 1.0, 2.5, 5.0, and 10.0 mass% CBPO with 10,000 ppm Fe, using ASTM E698 method

$$E = \left(\frac{-2.303R}{D} \right) \left[d \frac{\log_{10} \beta}{d(1/T)} \right] \tag{14}$$

Figure 6 shows the E_a value determination of 1.0, 2.5, 5.0, and 10.0 mass% CBPO with 10,000 ppm Cu, applying the ASTM E698 method. The E_a value of 10.0 mass% CBPO with 10,000 ppm Cu is 144.78 kJ mol⁻¹, which was comparable to the value of E_a obtained from the Friedman method and the FWO method. Generally, by four sets of experiments, the R^2 value of the fitting model was relatively reliable. Apart from various concentrated CBPOs with 10,000 ppm Fe, the E_a values were determined from 116.34 to 128.97 kJ mol⁻¹. The values of R^2 were fitted as 0.9655–0.9995. The credibility of the CBPO with 10,000 ppm Fe sets models has been improved after supported by using ASTM E698, as shown in Fig. 7.

Table 5 SADT determination (°C) for different lower concentrated CBPO with Cu for various packages

CBPO concentration/mass%	Package/kg						
	5.0	10.0	25.0	50.0	100.0	1000.0	5000.0
1.0	80.0	77.0	72.0	69.0	66.0	55.0	53.0
2.5	72.0	69.0	65.0	62.0	59.0	53.0	53.0
5.0	63.0	60.0	57.0	57.0	57.0	55.0	51.0
10.0	59.0	58.0	57.0	56.0	55.0	54.0	51.0

Table 6 SADT determination (°C) for different lower concentrated CBPO with Fe for various packages

CBPO concentration/mass%	Package/kg						
	5.0	10.0	25.0	50.0	100.0	1000.0	5000.0
1.0	91.0	77.0	71.0	67.0	63.0	53.0	52.0
2.5	69.0	66.0	62.0	59.0	58.0	49.0	47.0
5.0	59.0	59.0	59.0	56.0	56.0	49.0	46.0
10.0	59.0	56.0	56.0	51.0	51.0	49.0	46.0

Determination of self-accelerating decomposition temperature (SADT)

SADT can be understood from the data reordered by heat generation and heat release [33]. We selected the seven standard packages of CBPO in the industry for calculating the value of SADT. The SADT values can be determined using the concept of heat loss similarity, recommended by the United Nations test method H.4, the heat accumulation storage test. The heat loss per unit mass L ($\text{W kg}^{-1} \text{K}^{-1}$) can be easily calculated according to Eq. (15) [34].

$$L = \ln 2C_p t_{1/2}^{-1} \quad (15)$$

where C_p is the specific heat ($\text{J kg}^{-1} \text{K}^{-1}$); $t_{1/2}$ is the half-time of cooling (s). As presents in Table 5, the SADT for four concentrated CBPOs with 10,000 ppm Cu was calculated. As the lowest concentration (1.0 mass%) mixed with 10,000 ppm Cu in this study, the SADT value was 80.0 °C. With the package larger, the SADT value became opposite lower. Meanwhile, the SADT value also reduced, along with the concentration of CBPO being higher. When 10.0 mass% CBPO with 10,000 ppm Cu storage at the groove of 100 kg, the SADT value was inferred as 55.0 °C. For lower concentrated CBPO with 10,000 ppm Fe experiments, the SADT value was getting lower when the CBPO volume was getting higher. The range of four concentration CBPO with 10,000 ppm Fe was from 91.0 to 51.0 °C, as organized in Table 6.

Moreover, the reaction progress of various concentrated CBPOs with Cu/Fe at different isothermal conditions was simulated. Figure 8 revealed a reaction situation of 10.0 mass% mixed with 10,000 ppm Cu at five different isothermal conditions. The mixture of 10.0 mass% mixed with 10,000 ppm Cu would be completely reacted in just 25.1 h.

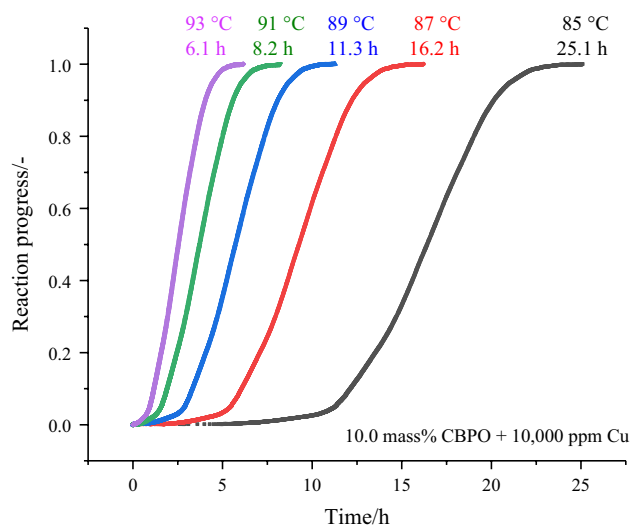


Fig. 8 TMR_{180} curves by reaction progress versus time for 10.0 mass% CBPO mixed with 10,000 ppm Cu at isothermal simulations

Conclusions

The heat flow examination results show that the reaction consumes time, and the maximum reaction rate would more significantly delay the heating rate. The DSC experiments results for CBPO mixed with Zn cannot precisely present the decomposition during heating because a crystallization reaction occurred during sample preparation. Using isoconverional kinetic analysis has excellent performance on the E_a and the R^2 determination of CBPO mixed with Cu/Fe at any reaction progress. On fitting of the kinetic model, ASTM E698 method calculation results were more accurate than that of the Kissinger method.

Whether mixed with Cu or Fe, the SADT values of different CBPOs were higher than pure CBPO, but the potential risk was still considerable.

Acknowledgements National Nature Science Foundation of China financially (Nos. 21927815 and 51574046) and National Key Research Development Program of China (No. 2019YFC0810701) supported this study.

References

1. Lin T, Zhang M, Xu F, Wang X, Xu Z, Guo L. Colorimetric detection of benzoyl peroxide based on the etching of silver nanoshells of Au@Ag nanorods. *Sens Actuators B*. 2018;261:379–84.
2. Lu KT, Chen TC, Hu KH. Investigation of the decomposition reaction and dust explosion characteristics of crystalline benzoyl peroxides. *J Hazard Mater*. 2009;161:246–56.
3. Huang AC, Chuang YK, Huang CF, Shu CM. Thermokinetic analysis of the stability of malic and salicylic acids in cosmeceutical formulations containing metal oxides. *J Therm Anal Calorim*. 2017;132:165–72.
4. Zhang Y, Chen R, Zhao M, Luo J, Feng W, Fan W, et al. Hazard evaluation of explosion venting behaviours for premixed hydrogen-air fuels with different bursting pressures. *Fuel*. 2020;268:117313.
5. Huang AC, Chen WC, Huang CF, Zhao JY, Deng J, Shu CM. Thermal stability simulations of 1,1-bis(tert-butylperoxy)-3,3,5-trimethylcyclohexane mixed with metal ions. *J Therm Anal Calorim*. 2017;130:949–57.
6. Liu SH, Hou HY, Shu CM. Thermal hazard evaluation of the autocatalytic reaction of benzoyl peroxide using DSC and TAM III. *Thermochim Acta*. 2015;605:68–76.
7. Cao CR, Liu SH, Das M, Shu CM. Evaluation for the thermokinetics of the autocatalytic reaction of cumene hydroperoxide mixed with phenol through isothermal approaches and simulations. *Process Saf Environ Prot*. 2018;117:426–38.
8. Cao CR, Liu SH, Huang AC, Lee MH, Ho SP, Yu WL, et al. Application of thermal ignition theory of di(2,4-dichlorobenzoyl) peroxide by kinetic-based curve fitting. *J Therm Anal Calorim*. 2018;133:753–61.
9. Huang AC, Huang CF, Xing ZX, Jiang JC, Shu CM. Thermal hazard assessment of the thermal stability of acne cosmeceutical therapy using advanced calorimetry technology. *Process Saf Environ Prot*. 2019;131:197–204.
10. Huang AC, Huang CF, Tang Y, Xing ZX, Jiang JC. Evaluation of multiple reactions in dilute benzoyl peroxide concentrations with additives using calorimetric technology. *J Loss Prev Process Ind*. 2021;69:104373.
11. Tan J, Bissonnette R, Gratton D, Kerrouche N, Canosa JM. The safety and efficacy of four different fixed combination regimens of adapalene 0.1%/benzoyl peroxide 2.5% gel for the treatment of acne vulgaris: results from a randomised controlled study. *Eur J Dermatol*. 2018;28:502–8.
12. Osman-Ponchet H, Sevin K, Gaborit A, Wagner N, Poncet M. Fixed-combination gels of adapalene and benzoyl peroxide provide optimal percutaneous absorption compared to monad formulations of these compounds: results from two in vitro studies. *Dermatol Ther (Heidelb)*. 2017;7:123–31.
13. You ML. Thermal hazard evaluation of cumene hydroperoxide-metal ion mixture using DSC, TAM III, and GC/MS. *Molecules*. 2016;21:562.
14. Duh YS. Chemical kinetics on thermal decompositions of cumene hydroperoxide in cumene studied by calorimetry: an overview. *Thermochim Acta*. 2016;637:102–9.
15. Wang Q, Liu SH, Huang AC, Huang CF, Chuang YK, Shu CM. Effects of mixing malic acid and salicylic acid with metal oxides in medium- to low-temperature isothermal conditions, as determined using the thermal activity monitor IV. *J Therm Anal Calorim*. 2018;133:779–84.
16. Wei M, Huang AC, Shu CM, Zhang L. Thermal decomposition and nonisothermal kinetics of monoethanolamine mixed with various metal ions. *Sci Rep*. 2019;9:1592.
17. Yang Y, Tsai YT, Zhang YN, Shu CM, Deng J. Inhibition of spontaneous combustion for different metamorphic degrees of coal using Zn/Mg/Al-CO₃ layered double hydroxides. *Process Saf Environ Prot*. 2018;113:401–12.
18. Tsai YT, Yang Y, Huang HC, Shu CM. Inhibitory effects of three chemical dust suppressants on nitrocellulose dust cloud explosion. *AIChE J*. 2020;66:e16888.
19. Tsai YT, Yang Y, Wang CP, Shu CM, Deng J. Comparison of the inhibition mechanisms of five types of inhibitors on spontaneous coal combustion. *Int J Energy Res*. 2018;42:1158–71.
20. Shiue GY, Huang AC, Chen JR. Thermal decomposition of triacetone triperoxide by differential scanning calorimetry. *J Therm Anal Calorim*. 2018;133:745–51.
21. Tsai YT, You ML, Qian XM, Shu CM. Calorimetric techniques combined with various thermokinetic models to evaluate incompatible hazard of tert-butyl peroxy-2-ethyl hexanoate mixed with metal ions. *Ind Eng Chem Res*. 2013;52:8206–15.
22. Vyazovkin S, Burnham AK, Criado JM, Pérez-Maqueda LA, Popescu C, Sbirrazzuoli N. ICTAC Kinetics Committee recommendations for performing kinetic computations on thermal analysis data. *Thermochim Acta*. 2011;520:1–19.
23. Vyazovkin S. Kissinger method in kinetics of materials: Things to beware and be aware of. *Molecules*. 2020;25:2813.
24. Liu SH, Cao CR, Lin WC, Shu CM. Experimental and numerical simulation study of the thermal hazards of four azo compounds. *J Hazard Mater*. 2019;365:164–77.
25. Deng J, Zhao JY, Huang AC, Zhang YN, Wang CP, Shu CM. Thermal behavior and microcharacterization analysis of second-oxidized coal. *J Therm Anal Calorim*. 2016;127:439–48.
26. Vyazovkin S, Sbirrazzuoli N. Isoconversional kinetic analysis of thermally stimulated processes in polymers. *Macromol Rapid Commun*. 2006;27:1515–32.
27. Laiwang B, Liu SH, Shu CM. Thermal hazards of benzoyl peroxide and its derived process products through theoretical thermodynamics assessment and different calorimetric technologies. *J Hazard Mater*. 2019;380:120891.
28. Wang J, Jia H, Tang Y, Xiong X, Ding L. Thermal stability and non-isothermal crystallization kinetics of metallocene poly(ethylene-butene-hexene)/high fluid polypropylene copolymer blends. *Thermochim Acta*. 2017;647:55–61.
29. Deng J, Zhao JY, Xiao Y, Zhang YN, Huang AC, Shu CM. Thermal analysis of the pyrolysis and oxidation behaviour of 1/3 coking coal. *J Therm Anal Calorim*. 2017;129:1779–86.
30. Akahira T, Sunose T. Method of determining activation deterioration constant of electrical insulating materials. *Res Rep Chiba Inst Technol (Sci Technol)*. 1971;16:22–31.
31. Xiao Y, Lü HF, Huang AC, Deng J, Shu CM. A new numerical method to predict the growth temperature of spontaneous combustion of 1/3 coking coal. *Appl Therm Eng*. 2018;131:221–9.
32. Laiwang B, Tsai YT, Liu SH, Deng J, Xiao Y, Wang QH, et al. Effects of 1-butyl-3-methylimidazolium nitrate on the thermal hazardous properties of lignitons and long flame coal through a green approach and thermokinetic models. *Process Saf Environ Prot*. 2019;131:127–34.

33. Zhang Y, Chung YH, Liu SH, Shu CM, Jiang JC. Analysis of thermal hazards of O, O-dimethylphosphoramidothioate by DSC, TG, VSP2, and GC/MS. *Thermochim Acta*. 2017;652:69–76.
34. Malow M, Michael-Schulz H, Wehrstedt KD. Evaluative comparison of two methods for SADT determination (UN H.1 and H.4). *J Loss Prev Process Ind*. 2010;23:740–4.

Publisher's Note Springer Nature remains neutral with regard to jurisdictional claims in published maps and institutional affiliations.